Key Engineering Materials
ISSN: 1662-9795, Vol. 1048, pp 121-132
doi:10.4028/p-TXaD32

Submitted: 2026-01-18
Revised: 2026-02-15
Accepted: 2026-02-23
Online: 2026-04-14

Detection of Charge Welds in Lateral Angular Co-Extrusion Using Non-Destructive Testing

Alexej Verschinin[1,a *], Florian Patrick Schäfke[1,b], Norman Mohnfeld [2,c]
Hans Jürgen Maier[1,d], Johanna Uhe[2,e], Christian Klose[1,f]
and Sebastian Barton[1,g]

[1]Leibniz University Hannover, Institut für Werkstoffkunde (Institute of Materials Science), 30823 Garbsen, Germany

[2]Leibniz University Hannover, Institut für Umformtechnik und Umformmaschinen (Institute of Forming Technology and Machines), 30823 Garbsen, Germany

[a]verschinin@iw.uni-hannover.de, [b]schaefke@iw.uni-hannover.de,
[c]mohnfeld@ifum.uni-hannover.de, [d]maier@iw.uni-hannover.de, [e]uhe@ifum.uni-hannover.de,
[f]klose@iw.uni-hannover.de, [g]barton@iw.uni-hannover.de

Keywords: lateral angular co-extrusion, charge welds, non-destructive testing

Abstract. Although extrusion is a well-established and widely used manufacturing process, charge weld seams remain a persistent challenge due to oxides, contaminants, and unfavorable material flow conditions at billet-to-billet transitions. In lateral angular co-extrusion (LACE), the material flow becomes more complex because it is redirected orthogonally to the ram movement and the metal is segmented into four separate streams in the die. This results in charge weld seams developing in more intricate shapes and locations than in conventional forward extrusion. Knowing the position of these seams along the profile is therefore essential for ensuring the structural integrity of co-extruded hybrid profiles, such as aluminum alloy hollow profiles reinforced by an inner titanium alloy tube. This study investigated the formation of charge weld seams in LACE through controlled billet-on-billet experiments. A hybrid profile was produced consisting of EN AW-6082 aluminum alloy as the lightweight component and a reinforcement element made of titanium grade 5 (Ti-6Al-4V). To enable accurate detection of the charge weld seam within the aluminum alloy part of the profile using non-destructive testing methods, a thin iron foil was inserted as a robust marker prior to extrusion between two parts of a split billet. Eddy-current testing (ET) and ultrasonic testing (UT) were applied to detect and map the charge weld seam along the extruded profile. ET enabled robust, high-resolution circumferential mapping of the weld propagation, while UT provided depth-resolved information. Complementary cross sections were prepared to validate the NDT results and characterize seam morphology. This combined approach provides a clearer picture of the formation of charge weld seams in LACE and demonstrates that NDT techniques can be used to reliably identify and assess these features in complex hybrid profiles.

Introduction

Charge welds, often referred to as transverse welds, occur during the extrusion of aluminum alloys at the interfaces of successive blocks and are therefore an inherent feature of the industrial extrusion process. Unlike longitudinal welds, these welds run transversely to the extrusion direction and can have a decisive influence on the local mechanical properties, fatigue strength, and failure behavior of profiles [1–3]. In addition to the weaker mechanical properties of charge welds, reduced corrosion resistance has also been reported [4].

The quality of such pressure welded joints depends significantly on process parameters such as ram speed, tool geometry, and degree of deformation, as well as on the microstructure and surface condition of the aluminum alloy billets used [5,6]. Impurities and oxide particles on the front surface of the billets can reduce the material properties of the charge welds [5,7].

Beyond the general influence of oxides and contamination, the local mechanical properties of charge welds also depend on their position and morphology along the weld path. At the weld nose

(the tip of the weld tongue), the properties are typically inferior, but they gradually transition toward those of the base material further along the weld path [8]. The number of weld tongues, and thus the number of charge weld interfaces, correlates directly with the number of portholes in the die. The increased complexity of material flow in asymmetric or multichannel dies makes it more difficult to predict the precise location of the weld noses, which in turn requires higher metallographic effort for their localization [8,9].

For these reasons, the position of charge welds, especially the weld nose(s), is of significant importance for the evaluation of materials and components, with non-destructive testing (NDT) methods offering potential support in this regard [9]. Engelhardt et al. investigated this issue and reported that, unlike longitudinal welds, the non-destructive detection of charge welds presents considerable challenges [10]. During eddy-current testing (ET), variations in electrical conductivity can serve as an indicator for longitudinal welds, provided that no recrystallisation has occurred. However, in charge welds, the conductivity difference relative to the base material is much smaller, making detection considerably more difficult. Additionally, the weld interface lies beneath the surface and is not oriented orthogonally as it is with longitudinal welds [10].

Ultrasonic testing (UT) is suitable for detecting longitudinal and transverse (charge) welds, as it is sensitive to changes in microstructure and inhomogeneities [9]. Zhao demonstrated the detection of longitudinal welds in extruded 6xxx-series aluminum alloys by mapping attenuation properties arising from differences in grain size relative to the base material [11]. However, in the present context, UT is of limited practical relevance as it depends strongly on acoustic coupling and correct handling, making it more suitable as a laboratory method than for industrial application [10]. In particular, the sound path must be precisely controlled in order to reliably assess grain size or material inhomogeneities [12], an aspect that poses considerable challenges for in-line inspection.

To address these challenges, a method was developed in the present study to enable precise localization and characterization of charge welds in LACE profiles. During billet-to-billet extrusion, a thin iron foil was placed between two billets to mark the charge weld interface. Owing to its ferromagnetic properties, the iron foil provides high contrast with aluminum in eddy-current testing, enabling reliable detection of the circumferential propagation of the charge weld. In addition, the interlayer creates favorable conditions for ultrasonic testing, allowing depth-resolved information to be obtained.

Specifically, the aim of the present study was to localize and characterize charge welds in LACE profiles using ET and UT, and to compare the capabilities of both methods in resolving weld position, circumferential propagation, and depth.

Materials, Experiments, and Test Procedures

Extrusion. The extrusion tests carried out were aimed at the controlled production of charge welds in the LACE process as this process is characterized by a complex material flow inside the tool. The tests were performed on a 10 MN extrusion press (SMS Meer GmbH, Düsseldorf, Germany). The LACE tool used is shown schematically in Fig. 1. The material flow within the tool has been described in detail by Thürer et al. [13]. Billets made of the aluminum alloy EN AW-6082 and reinforcement tubes made of Ti-6Al-4V (titanium grade 5) were used as joining partners. The container diameter was 146 mm, the die opening was 62.7 mm, and the titanium alloy tubes had an outer diameter of 44.5 mm. This resulted in an extrusion ratio of approximately 11:1.

To promote metallic bonding by friction between EN AW-6082 and Ti-6Al-4V in the extrusion process, the surface of the titanium alloy tube was roughened with 40-grit emery paper directly before the trials and then cleaned with ethanol. The EN AW-6082 billets were preheated to 530 °C for 4.5 hours, while the titanium grade 5 tube was at room temperature at the start of each test and only heated up upon insertion into the preheated LACE tool. The LACE tool and the container were heated to 490 °C and 440 °C, respectively. At the start of extrusion, a ram speed of 1.5 mm/s was set during the upsetting of the billet in the container and the filling of the LACE tool in order to minimize the cooling of the aluminum alloy billet during tool filling. The ram speed was then gradually reduced to the target speed for composite formation of 0.3 mm/s.

To create a defined charge weld seam, two EN AW-6082 billets, 100 mm and 200 mm long, were loaded into the container in series, with the 100 mm billet placed adjacent to the extrusion die and the 200 mm billet behind it, so that the 100 mm billet entered the die first. Two test variants using such split billets were conducted: (i) with a 0.05 mm thin unalloyed iron foil inserted at the interface between the two EN AW-6082 billets (see Fig. 2a), and (ii) without an iron foil, such that only the natural oxide layer and the saw-cut surface acted as the separating layer during formation of the charge weld seam.

A third LACE profile from a previous study, manufactured under identical parameters and using the same materials but without splitting the billet, served as the reference for the ET examination.

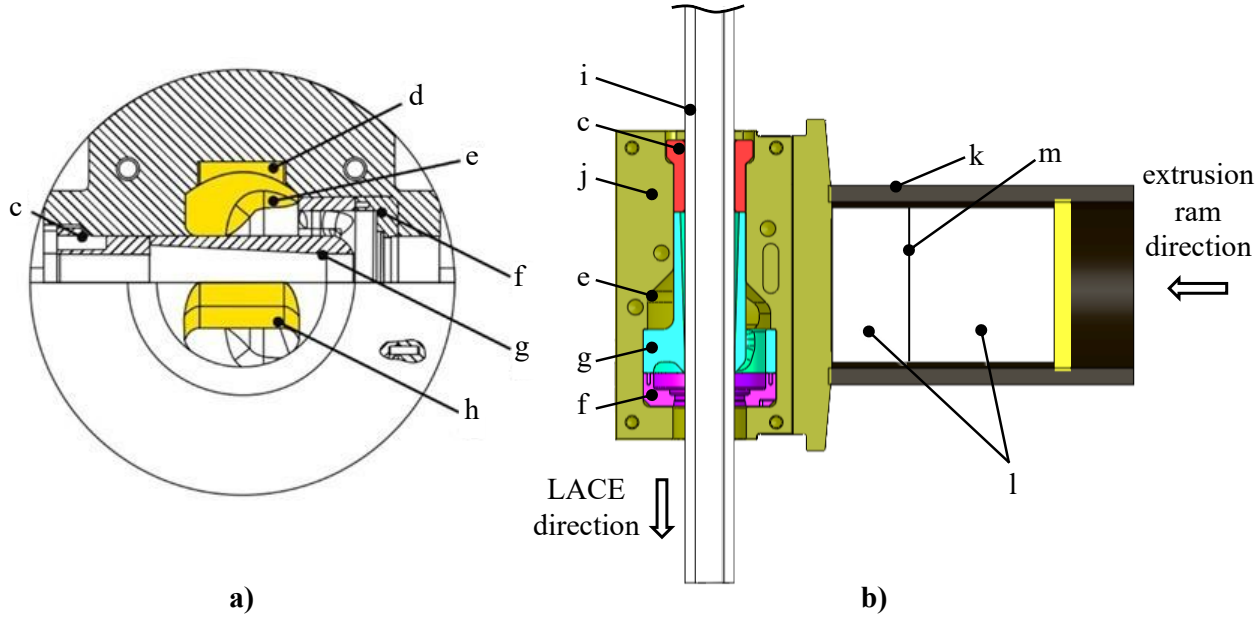

Fig. 1. Illustration of the LACE tool; (a) Schematic illustration with sectional plane lengthwise through the tool [13], with c: clamping cover, d: pocket, e: deflection, f: die, g: mandrel part with three support arms, h: inlet (the geometry of the inlet and deflection are highlighted);
(b) schematic illustration of the concept for the 10 MN extrusion press in longitudinal section with i: reinforcing element (titanium grade 5 tube), j: die housing, k: container, l: EN AW-6082 split billet, m: iron foil.

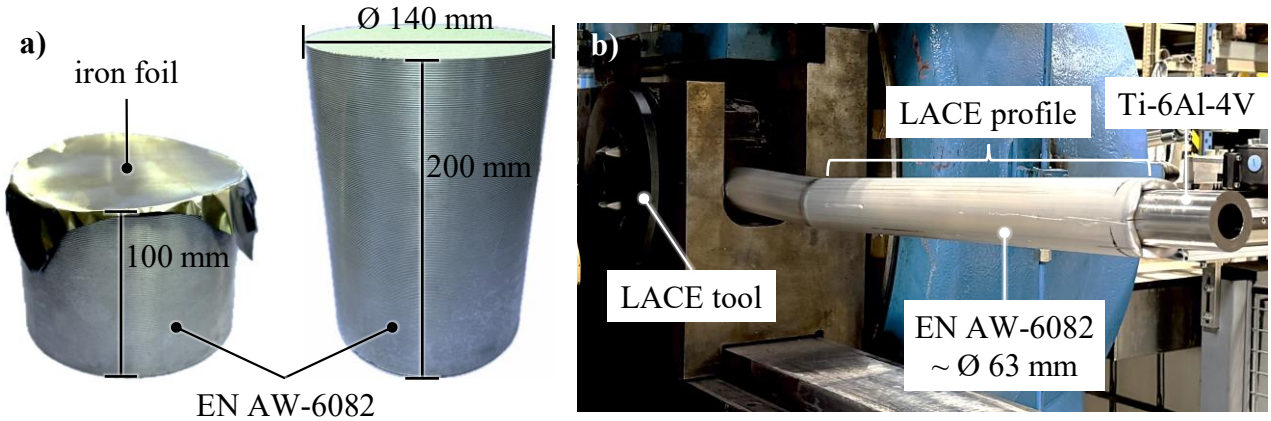

Fig. 2. (a) The aluminum alloy billets with the iron foil placed on top of the 100 mm-long billet; (b) the LACE profile after extrusion.

The press diagram in Fig. 3 shows the ram force curve for the extrusion test with iron foil in red and without iron foil in yellow. The corresponding ram speeds are shown in black and gray. In the time

interval from 0 to 120 s, the upsetting of the billet and the filling of the LACE tool at ram speeds between 1.5 mm/s and 0.3 mm/s can be observed. In the time interval from 120 s to approx. 300 s, the aluminum alloy was extruded around the titanium alloy tube inside the die. At approx. 300 s, a sharp decrease in the ram force marks the end of the titanium alloy tube leaving the mandrel part of the LACE tool, after which only aluminum alloy, without reinforcement element, was extruded. After extrusion, the LACE profile cooled down in ambient air. The data in Fig. 3 show that the ram force differed only minimally in both experiments, and based on the curves, the influence of the iron foil on the material flow is negligible, and the charge welds will have formed similarly as a result. A LACE profile produced with an iron foil between the billets is shown in Fig. 2b. Neither the charge welds nor the iron foil were visible on the profile surface.

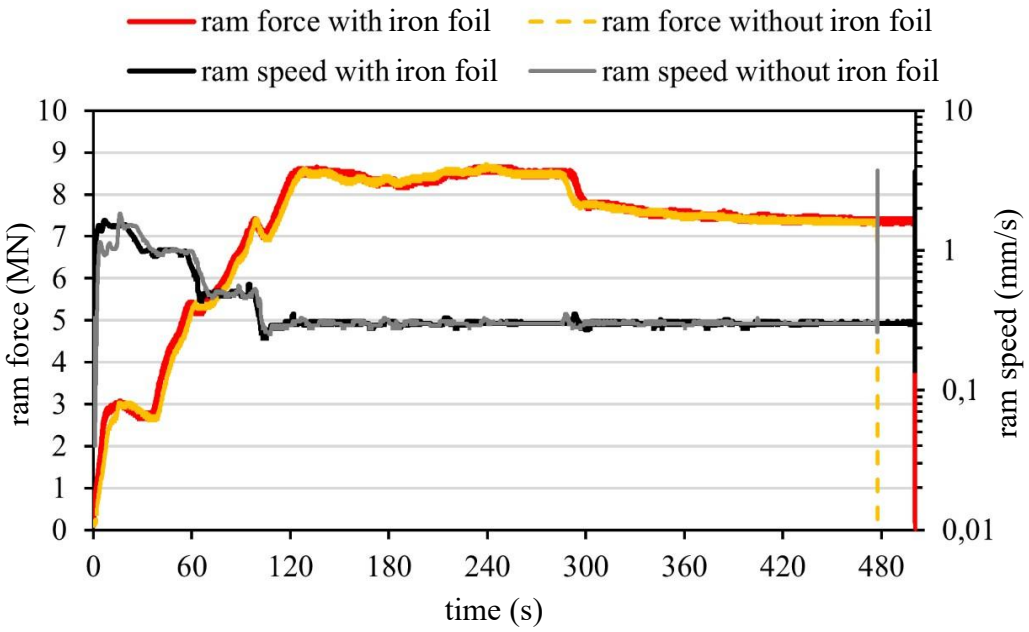

Fig. 3. Press diagram with force and ram speed for the two press trials

Non-destructive testing. In order to achieve precise positioning of the sensors, the NDT measurements were conducted utilizing an automated test rig. It was equipped with a linear and a rotational drive, which were controlled via an axis control unit (Isel Germany GmbH, Eichenzell, Germany), shown in Fig. 4a.

For the ET, an absolute eddy-current sensor developed in-house and dedicated testing software were utilized. The measurements were performed automatically as line scans along the longitudinal axis of the profile, with rotational steps of 10° around its circumference, following the axis definitions illustrated in Fig. 4.

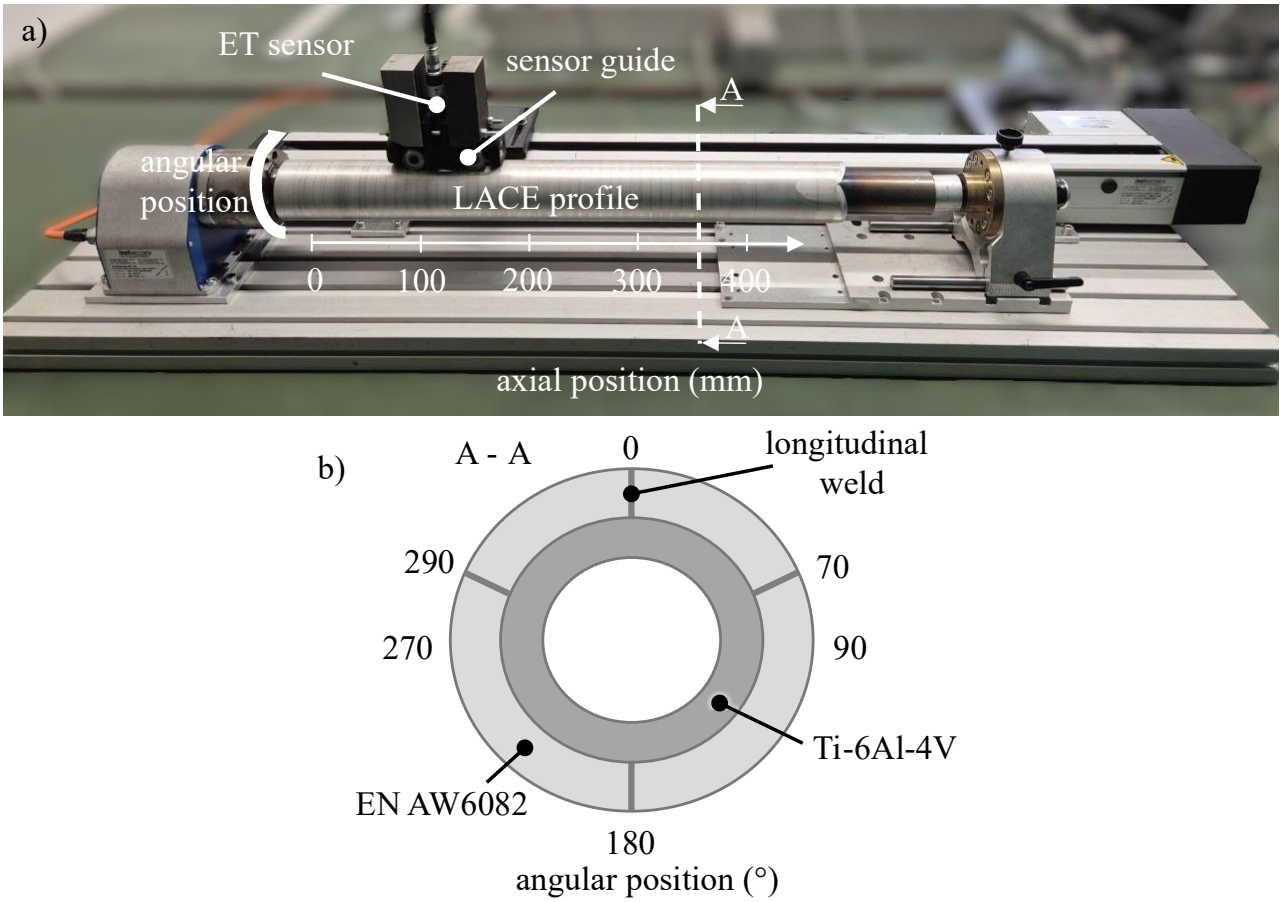

Fig. 4. (a) NDT test rig equipped with ET sensor and (b) schematic cross section of a LACE profile

The primary parameter varied was the testing frequency; 200 Hz, 1 kHz, and 10 kHz were selected to achieve increased penetration depths with decreasing frequency. The penetration depth δ was calculated according to

$$\delta = \frac{1}{\sqrt{\pi f \mu \sigma}} \quad (1)$$

with

f – EC testing frequency; μ – magnetic permeability and σ – electrical conductivity of the material.

The phase was tuned to align the lift-off effect predominantly with the real component, thereby isolating the measurement effect within the imaginary component. The remaining parameters (pre-gain, gain, and source) were configured to maximize the signal difference between reference samples and the EN AW-6082 specimens with differing electrical conductivities, while preventing excessive noise from dominating the measurement.

During post-processing, the raw numerical data of the imaginary component from each line scan were smoothed using a Savitzky–Golay filter, reducing the data to one point per millimeter. The data were subsequently normalized for each measurement run. The resulting data were further processed into a heatmap, with the profile length represented on the x-axis and the circumference on the y-axis (Fig. 5).

The ultrasonic testing was carried out using a Krautkrämer USLT 2000 device (GE Sensing & Inspection Technologies GmbH, Wunstorf, Germany). A 5 mm pulse-echo transducer operating at 15 MHz was employed for the ultrasonic measurements. The transducer was equipped with a spacer and used in combination with Krautkrämer ZG-F as the ultrasonic couplant. This configuration was chosen to enhance defect sensitivity and to shift the focal region toward shallow depths. To ensure

optimal acoustic coupling, the measurements were conducted semi-automatically on the previously described test bench, following a mesh of 30° and 10 mm steps across the LACE profile.

The raw data that have been acquired consisted of ultrasonic A-scans, representing amplitude as a function of sound propagation distance. Consecutive A-scans were then assembled into color-encoded B-scans, which represent the depth-resolved signal variation along the scanning path. C-scans were then generated by extracting the signal amplitude within a predefined depth window, corresponding to the expected echo location, and mapping these values onto a two-dimensional view of the inspected area.

Cross-section preparation. After the NDT inspection, the profile with iron foil was sectioned by water-jet cutting at the axial positions of 320 mm, 280 mm, 240 mm and 200 mm, and at the angular positions of 0° and 180°, resulting in four cross-sections of 180° each. These sections were subsequently ground using abrasive papers up to 800 grit to enhance the visibility of the iron foil. The prepared cross-sections were then photographed and evaluated using image analysis software ImageJ.

Results

Eddy current testing. To illustrate the previously mentioned challenges of detecting charge welds using ET, two LACE profiles, one with and one without a charge weld and neither containing any marker material, were evaluated (Fig. 5). With a testing frequency of 200 Hz, an estimated penetration depth of 6.8 mm was achieved.

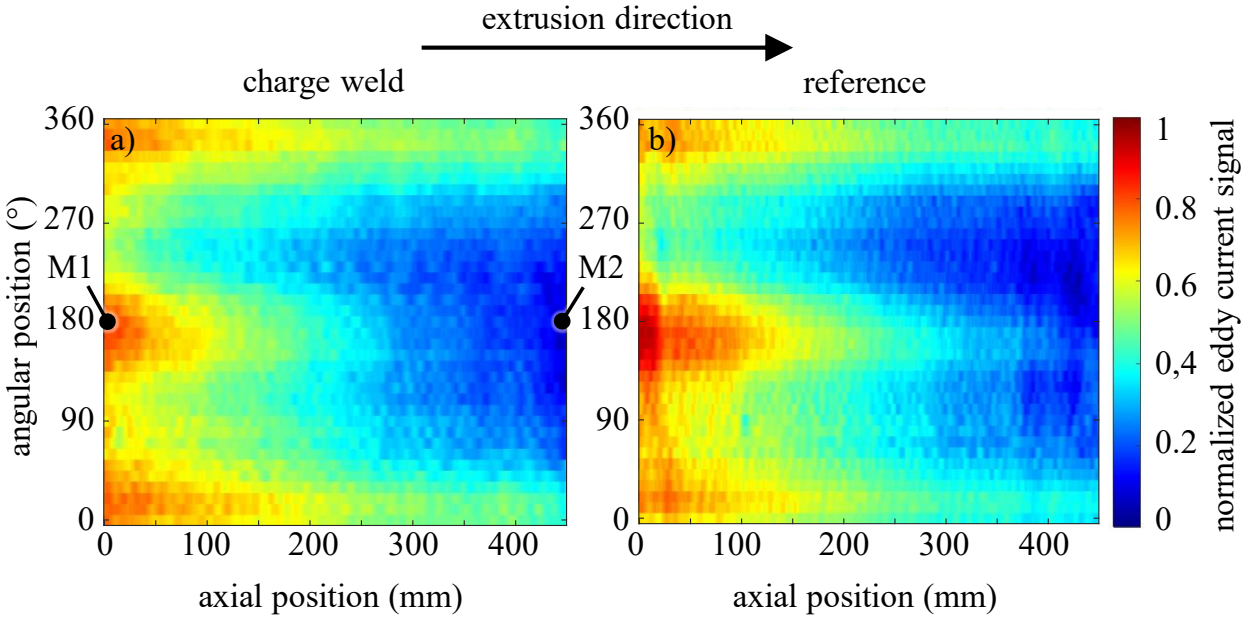

Fig. 5. ET heatmaps of LACE profiles with (a) and without (b) charge welds (testing frequency 200 Hz)

As assumed, no structures resembling charge welds were visible. Apparently, the conductivity-changing factors that typically occur during a conventional billet change, such as dwelling of the remaining material from the first billet in the die, resulting in differing local heat treatment and oxide contamination, were absent in the present split-billet setup.

However, the heatmaps already revealed some of the profile's characteristic features. The signal amplitude decreased along the profile axis. This behavior was consistently observed in all LACE profiles investigated so far. This behavior was presumably caused by the profiles remaining attached to the LACE tool after extrusion for cooling before being separated by a bandsaw, so that regions located closer to the LACE tool were exposed to higher temperatures for a longer time than regions further away. This likely resulted in different states of artificial aging, which in turn affected the electrical conductivity [15]. A correlation between the signal amplitude and electrical conductivity on LACE profiles has previously been established using a commercially available electrical

conductivity meter. In the present case, for example, the electrical conductivities measured at positions M1 and M2 (as shown in Fig. 5) were 31.2 MS/m and 29.2 MS/m, respectively.

Considering the variation of the signal amplitude around the circumference, it became apparent that it had its maxima at approximately 0°/360° and 180°, which can likely be attributed to the influence of the formation of two of the four longitudinal welds.

These measurements served as a baseline and highlighted the limited intrinsic contrast the ET signals provided for the charge welds under the present conditions. Hence, the iron foil was used as an electromagnetic marker during extrusion to enhance the detectability of the charge weld.

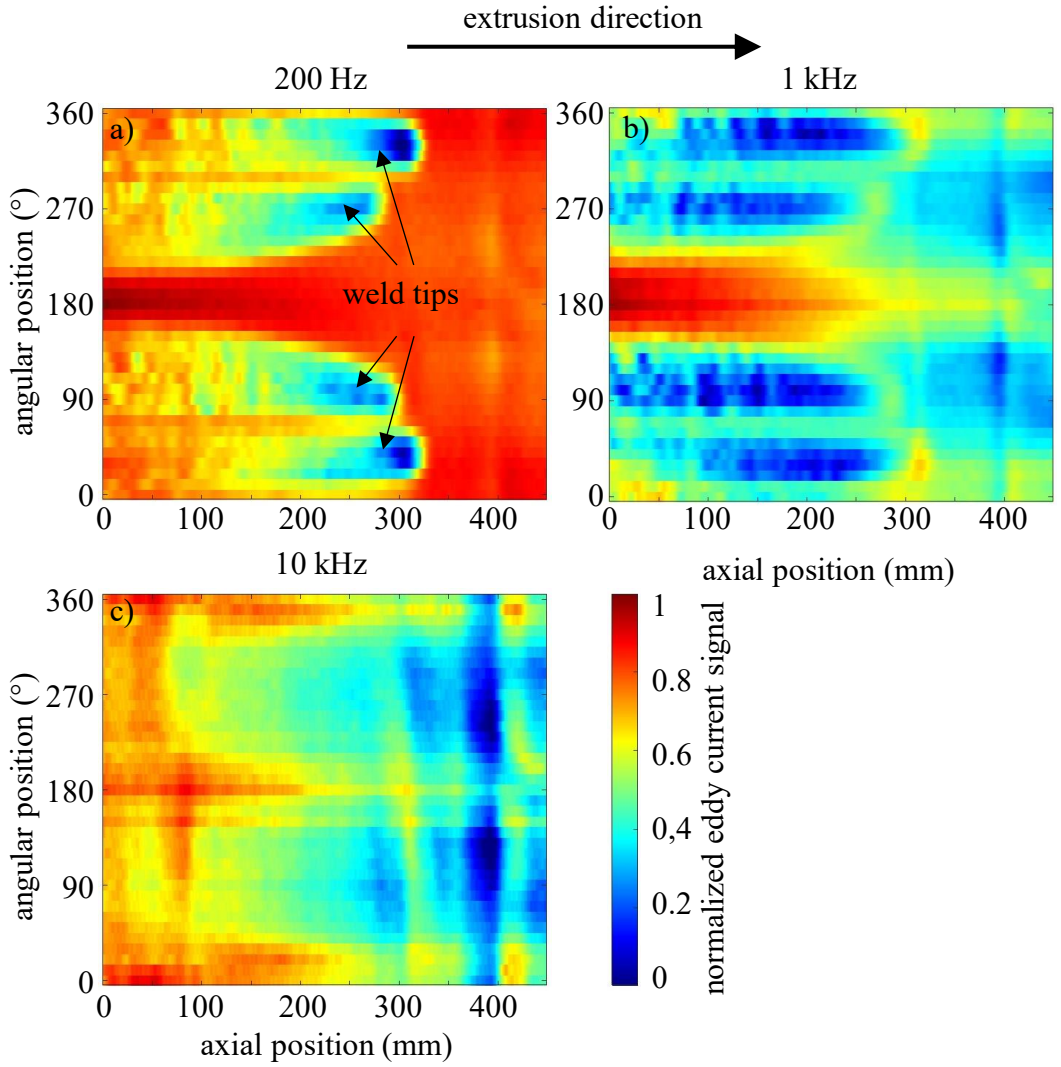

Fig. 6. ET heatmaps of the LACE profile with iron foil conducted at different testing frequencies

Following the evaluation of LACE profiles without any marker material, the iron foil experiments were used to provide a high-contrast reference for mapping the charge weld geometry. Fig. 6 shows heatmaps of the ET response obtained at different testing frequencies. Each frequency provided information from a distinct penetration depth. At lower testing frequencies of 200 Hz and 1 kHz with approximate penetration depths of 6.8 mm and 3.04 mm respectively, the distribution patterns of the charge welds became apparent. The weld tips were located at angles of approximately 30-40°, 90°, 270° and 330° around the circumference, as well as at axial positions of around 320 mm, 290 mm and 280 mm, as shown in Fig. 6a.

As extrusion progressed, the subsequent billet displaced the preceding billet, thereby widening the cross-section of the charge weld [9]. This behavior was observed in Fig. 6a, where the weld occupied a progressively larger portion of the circumference with increasing distance from the weld tip. Furthermore, the comparison of Fig. 6a and Fig. 6b shows a shift of the signal response with

progressing extrusion, which meant a shift of the upper weld interface towards shallower depths. This was accompanied by a progressive weakening of the signal response, which can be explained by the increasing expansion of the original contact area with increasing distance from the weld tip [8]. This generally results in a reduced amount of iron present per unit area and therefore in a weaker signal response.

At the highest ET frequency of 10 kHz (Fig. 6c), which is sensitive to the near-surface region down to approximately 0.96 mm, no features indicative of the charge weld could be detected. As a result, the heatmap mainly highlighted longitudinal welds and the axial conductivity trend rather than the charge weld itself.

Ultrasonic testing. In addition to the ET heatmaps, the UT C-scan also provided information on the areal distribution of charge welds across the LACE profile. The weld tips were identified in Fig. 7 at positions similar to those shown in the ET heatmaps, angularly at 30°, 90°, 270° and 330°, and axially at 320 mm, 300 mm and 280 mm. However, the circumferential spreading of the charge weld was poorly represented, largely due to the lower in-plane resolution resulting from the chosen semi-automatic measurement procedure rather than an inherent limitation of the UT method.

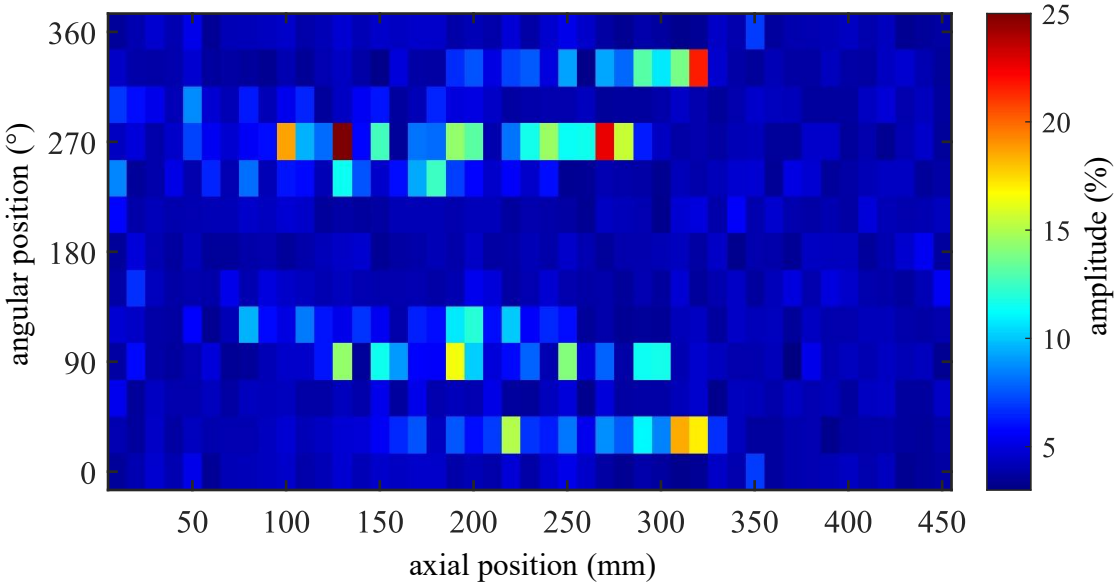

Fig. 7. UT C-scan of the LACE profile with iron foil (depth window 2.2 to 8 mm)

Furthermore, the signal response weakened with increasing distance from the weld tip, although this attenuation occurred more rapidly in UT. While ET still showed distinct signal amplitudes at an axial length of more than 300 mm, UT only detected weld-related indications within approximately 100-170 mm. This behavior can be explained by the fact that, below a depth of approximately 2.2 mm, reflections from the iron containing areas merge with the coupling echo from the surface. This coupling echo is relatively broad due to the curved surface of the specimen, thereby imposing a lower limit on the effective detection window.

Additional insight into the depth distribution of these indications was obtained from the UT B-scans. The scans, presented in Fig. 8, corresponded to axial positions of 320 mm, 280 mm, 240 mm and 200 mm, matching the locations of the respective cross-sections. On the left side of each B-scan, the amplitude of the coupling echo is visible. On the right side, the interface between the two materials appears as a wavy feature because the thickness of the aluminum alloy layer varies across the circumference in the unmachined profile (approximately 9 ± 1 mm). Between these two boundaries, indications caused by the iron foil remnants were identified.

The scans provided a cross-section through the charge welds located directly adjacent to the weld tip at the axial position of 320 mm and the angular positions of 30° and 330°. A similar pattern emerged at 280 mm, where the weld tips at 90° and 270° became visible. As extrusion progressed,

the indications moved apart and shifted toward both the surface and the material interface until they were masked by the amplitudes of the coupling echo and the interface reflection. Additionally, weaker amplitude signals emerged at 120° and 240°, indicating circumferential propagation of the weld.

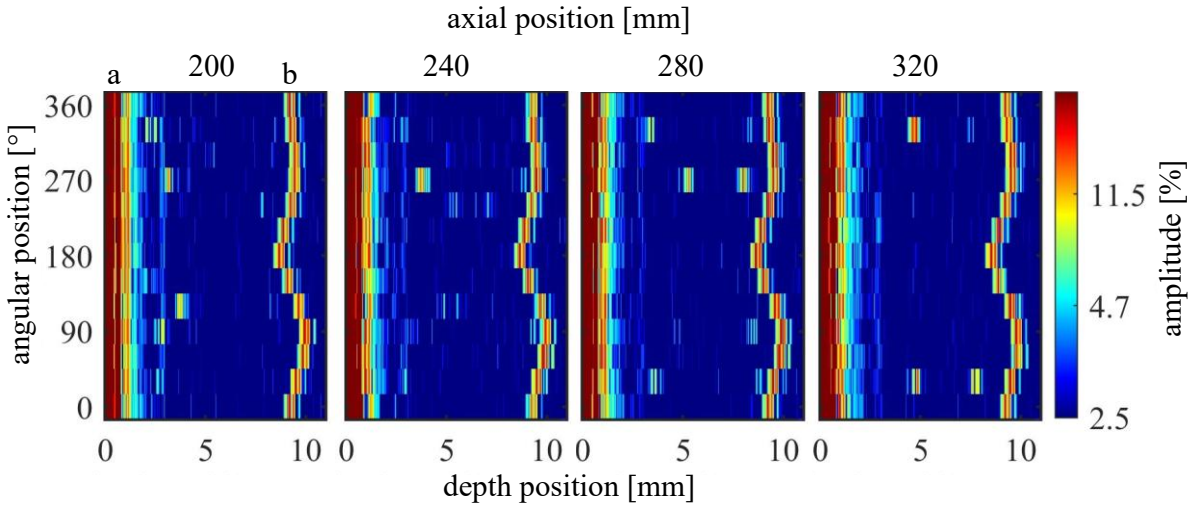

Fig. 8. UT B-scans at the axial positions corresponding to the cross-sections, (a) coupling echo representing the outer surface, (b) interface echo marking the joint between the aluminum alloy and titanium alloy parts

Optical analysis of the cross sections. The inserted iron foil provided high contrast in the cross-sections of the LACE profile, enabling clear optical insight into the formation of the charge welds. At the positions (320 mm / 330°) and (280 mm / 270°), welds were observed to be cut directly next to the weld tip, exhibiting nearly gapless contours. With progressing extrusion, the area enclosed by the weld expanded rapidly at first and slowed down at later stages, accompanied by a decrease in visible iron remnants, which is consistent with the described behavior of increasing area expansion with growing distance from the weld tip [8].

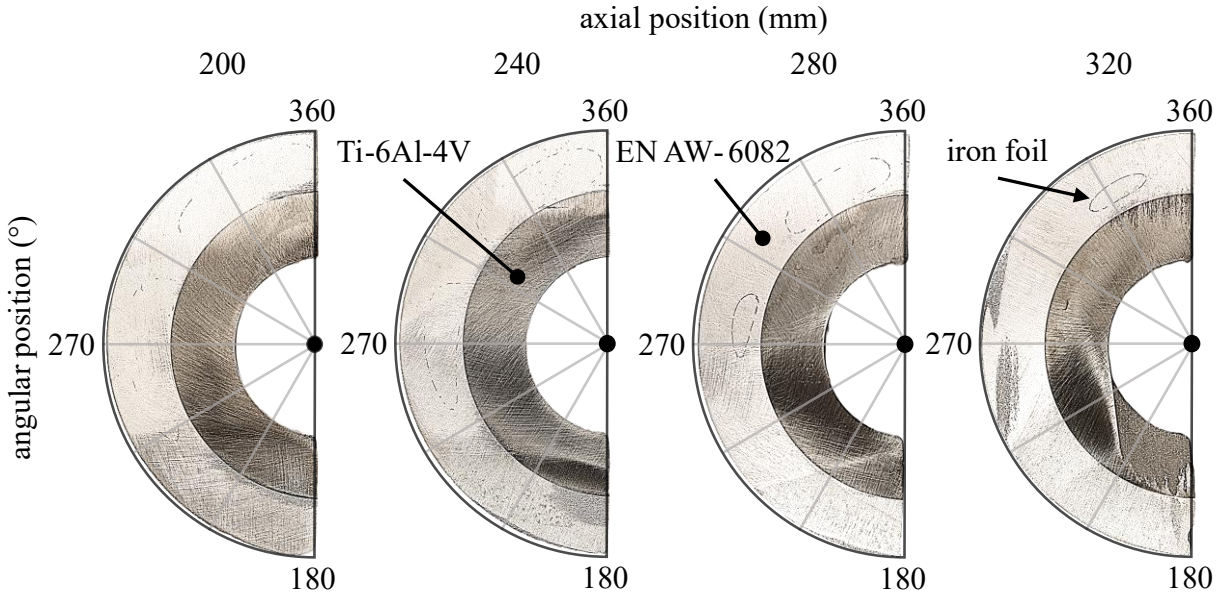

Fig. 9. Cross sections of the LACE profile with iron foil

To validate the ET and UT measurements, the prepared cross-sections, serving as the metallographic reference, were quantitatively evaluated. It should be emphasized that this comparison did not aim to assess the metrological accuracy of the applied NDT techniques in terms of statistical precision or resolution limits. Rather, the objective was to confirm the reliable detection of the charge

weld and its macroscopic localization within the component by correlating the NDT indications with the metallographic findings.

For this purpose, both the radial extent of the charge welds and their penetration depth were determined from the cross-sections at angular positions of 270° and 330°. The corresponding depth values obtained by UT were extracted from the B-scans, while the radial extent detected by ET was derived from the respective heatmaps. The results are summarized in Table 1.

Table 1. Comparison of charge weld position data obtained from cross-sections, ET, and UT

ax. pos. [mm]	depth [mm]		angle [°]	
	cross sections	UT	cross sections	ET
300	4.6 - 7.1	4.6 - 7.5	322 - 344	310 - 350
280	3.6 - 8.1	3.3 - 8.4	314 - 355	310 - 350
	5.0 - 7.1	5.3 - 7.9	263 - 287	260 - 290
240	3.1 - 8.9	2.8 – n/a	310 - 357	310 - 360
	3.7 - 8.4	3.7 – 9.0	246 - 292	240 - 290
200	2.5 - 8.9	2.1 - 8.5	309 - 360	310 - 360
	2.4 - 8.2	3.1 - n/a	234 - 293	230 - 290

Depth information was evaluated exclusively on the basis of UT results, as ET provides only indirect and frequency-dependent depth indications unless extensive calibration with suitable reference specimens is performed. In the present study, ET therefore allowed only a coarse assignment to depth ranges, whereas UT enabled a direct determination of the reflector position via time-of-flight analysis. However, practical factors must be considered, such as the geometry and spatial orientation of the reflector, and slight probe tilt angles due to the curved surface, which may alter the effective sound path length and lead to apparent depth shifts. In addition, detectability in the near-surface region is limited by the coupling echo, although this can be mitigated by optimized probe configurations such as dual-element transducers. Furthermore, iron remnants on the shallow side of the charge weld partially shielded the sound path, reducing the detectability of the deeper weld flank. Despite these constraints, the localization of the weld depth showed good agreement with the metallographic reference. The mean deviation was 0.27 mm for the upper weld interface and 0.5 mm for the lower weld interface.

The situation differs when considering the radial and axial propagation of the charge weld. The positional accuracy in this case was largely dependent on the applied scan mesh. Due to apparatus-related constraints, a finer circumferential mesh was used for ET, resulting in a mean angular deviation of 3.7°, whereas UT was performed with coarser angular increments. Beyond this mesh-dependent resolution, the detectability of the charge weld by UT was additionally influenced by the microstructural configuration. The cross-sections indicate that, as extrusion progressed, increasing gaps formed between the iron remnants. Moreover, toward the lateral regions of the charge weld, the particle interfaces become progressively aligned more parallel to the incident sound direction. Under such conditions, the reflected ultrasonic energy is reduced or redirected away from the probe, and the sound wave may pass the interface without generating a distinct echo, resulting in locally reduced detectability and signal loss toward the weld edges. Nevertheless, the weld tips were reliably localized by both NDT methods at measurement positions 320 mm/330° and 280 mm/270°, showing good qualitative agreement with the metallographic reference and confirming the practical suitability of both techniques for macroscopic weld localization.

Conclusions

ET and UT were successfully applied to detect marked charge welds in LACE profiles. ET enabled reliable circumferential mapping of the weld region, whereas UT provided depth-resolved information based on time-of-flight analysis. While ET is limited in penetration depth, UT is more

susceptible to reflector orientation, acoustic shadowing, and reduced sensitivity near the surface. Table 2 summarizes the key characteristics of the applied NDT techniques in the context of the investigated application.

Table 2. Comparison ET and UT for detection of marked charge welds in LACE profiles

criterion	UT	ET
physical principle	acoustic reflection at interfaces	electromagnetic property variation
inspection character	surface/interface detection along sound path	volumetric interaction within penetration depth
penetration depth	high	limited (frequency-dependent)
depth information	direct (time-of-flight)	indirect (frequency-based)
sensitivity to orientation	high	low
near-surface capability	limited (coupling echo)	high
contact requirement	requires acoustic coupling	no surface contact required

The choice of method depends on whether depth-related information or spatial weld propagation is of primary interest. However, for a comprehensive assessment of charge weld geometry, the combined use of both techniques is recommended.

However, charge welds could not be detected by ET in profiles without marker material in the application case presented. Under the present extrusion conditions, the conductivity variations required for detection, for example those arising from differing thermal exposure during a conventional billet change, could not be generated and therefore did not provide a detectable contrast.

Further work will focus on developing strategies for marker-free detection of charge welds in LACE profiles. In this context, multi-frequency ET is a promising approach, provided a measurable conductivity contrast can be established at the charge weld.

Acknowledgements

Funded by the Deutsche Forschungsgemeinschaft (DFG, German Research Foundation) – SFB 1153 TP A01 - 252662854.

References

[1] A. Bakker, L. Katgerman, S.d. Zwaag, Analysis of the structure and resulting mechanical properties of aluminum extrusions containing a charge weld interface, Journal of Materials Processing Technology 229 (2016) 9–21.

[2] Q. Li, C. Harris, M.R. Jolly, Finite element modelling simulation of transverse welding phenomenon in aluminum extrusion process, Materials & Design 24 (2003) 493–496.

[3] N. Nanninga, C. White, R. Dickson, Charge Weld Effects on High Cycle Fatigue Behavior of a Hollow Extruded AA6082 Profile, Journal of Materials Engineering and Performance 20 (2011) 1235–1241.

[4] J. Yu, G. Zhao, X. Zhao, L. Chen, M. Chen, Microstructures of longitudinal/transverse welds and back-end defects and their influences on the corrosion resistance and mechanical properties of aluminum alloy extrusion profiles, Journal of Materials Processing Technology 267 (2019) 1–16.

[5] A.J. den Bakker, R.J. Werkhoven, W.H. Sillekens, L. Katgerman, The origin of weld seam defects related to metal flow in the hot extrusion of aluminum alloys EN AW-6060 and EN AW-6082, Journal of Materials Processing Technology 214 (2014) 2349–2358.

[6] L. Donati, L. Tomesani, The prediction of seam welds quality in aluminum extrusion, Journal of Materials Processing Technology 153-154 (2004) 366–373.

[7] E.C. Sariyarlioglu, T. Welo, J. Ma, On the mechanisms of charge weld evolution in aluminum extrusion, Journal of Manufacturing Processes 124 (2024) 377–384.

[8] G. Oberhausen, D.R. Cooper, D.R. Cooper, Modeling the Strength of Aluminum Extrusion Transverse Welds Using the Film Theory of Solid-State Welding, 2023.

[9] A.J. den Bakker, Weld Seams in Aluminum Alloy Extrusions, Delft University of Technology.

[10] M. Engelhardt, D. Behne, N. Grittner, A. Neumann, W. Reimche, C. Klose, Non-destructive Testing of Longitudinal and Charge Weld Seams in Extruded Aluminum and Magnesium Profiles, Materials Today: Proceedings 2 (2015) 4866–4873.

[11] X. Zhao, T. Gang, X. Liu, S. Li, Application of ultrasonic non-destructive characterisation on materials' quality evaluation, Insight - Non-Destructive Testing and Condition Monitoring 52 (2010) 206–209.

[12] J. Krautkrämer, Ultrasonic Testing of Materials, fourth Fully Revised Edition, Springer, Berlin, Heidelberg, 1990.

[13] S.E. Thürer, J. Peddinghaus, N. Heimes, F.C. Bayram, B. Bal, J. Uhe, B.-A. Behrens, H.J. Maier, C. Klose, Lateral Angular Co-Extrusion: Geometrical and Mechanical Properties of Compound Profiles, Metals 10 (2020) 1162.

[14] P. Stucky, W. Lord, Skin Depth Considerations in Eddy Current NDT, in: D.O. Thompson, D.E. Chimenti (Eds.), Review of Progress in Quantitative Nondestructive Evaluation, Springer Science, New York, 1992, pp. 299–306.

[15] C. Li, C.D. Marioara, C. Hatzoglou, S.J. Andersen, R. Holmestad, Y. Li, Accelerating precipitation hardening by natural aging in a 6082 Al-Mg-Si alloy, Acta Materialia 281 (2024) 120396.

The publication of this article was funded by the Leibniz Universität Hannover (LUH) / Technische Informationsbibliothek (TIB)